PAPER

Check for updates

Polylactic acid based Janus membranes with asymmetric wettability for directional moisture transport with enhanced UV protective capabilities†

Yingshu Gu, Jing Wu, [ID] * Miaomiao Hu, Haohong Pi, Rui Wang [ID] and Xiuqin Zhang [ID] *

Efficient directional moisture transport can remove excess sweat away from the human body and keep the body dry; fully utilizing this functionality to improve the wearing experience is urgently needed in the area of functional textiles. Herein, a facile strategy is used to design an eco-friendly and biodegradable PLA membrane with enhanced directional moisture transport and UV protection abilities. The PLA-based Janus membrane with asymmetric wettability is fabricated *via* sol–gel and electrospinning methods. Titanium dioxide nanoparticles (TiO_2) were anchored onto the surface of the PLA fabric during the TiO_2 sol–gel fabrication process using polydopamine, forming superhydrophilic TiO_2@PDA–PLA. Then a thin PLA fibrous membrane layer showing hydrophobicity was electrospun onto this (PLA-E). The Janus PLA-E/TiO_2@PDA–PLA membrane was successfully fabricated. Due to the asymmetric wettability and anchored TiO_2, the PLA-E/TiO_2@PDA–PLA Janus membrane exhibits efficient directional moisture transport and excellent UV protection abilities, and this work may provide a new pathway for fabricating multifunctional personal protective materials and have attractive potential applications in the future.

Introduction

The production of multifunctional fabrics that can address special needs, such as flame-retardant fabrics, electromagnetic-interference-shielding fabrics, UV-protective fabrics, *etc.*, is increasingly demanded for use in people's daily lives.[1–4] Fabrics with directional moisture transport, which can remove excess sweat away from human skin to the environment and have a pivotal role in providing specific functionality, meeting comfort requirements by keeping the body dry, have received extensive attention in recent years.[5–7] Accordingly, the generation of asymmetric wettability between the two sides of the fabric is one of the more efficient and fascinating ways to realize directional moisture transport capabilities; membranes or fabrics exhibiting hydrophobicity on one side and hydrophilicity on the other side are referred to as Janus membranes.[8,9] For example, Cao *et al.* reported a binary cooperative Janus fog collector constructed from hydrophobic copper mesh and a superhydrophilic cotton absorbent, demonstrating enhanced fog-harvesting efficiency.[10] Dai *et al.* fabricated a hydrophobic/

superhydrophilic polyester/nitrocellulose textile with asymmetric hydrophilic conical micropores for directional water transport *via* a simple laser perforation method. The polyester/nitrocellulose textile can unidirectionally pump excess sweat from the hydrophobic layer to the superhydrophilic layer, thereby avoiding undesirable sticky and uncomfortable sensations arising from the presence of sweat.[11] Meanwhile, Janus membranes exhibiting unidirectional water transport or the penetration of tiny water droplets, which have been used as "water diodes" or for plant cultivation, were also developed by our group.[12–14] If the construction concepts used for Janus membranes were used for wearable fabrics, endowing excellent breathability and promoting the comfort of clothes, the resulting fabrics may serve as good candidates for use in the development of a secondary protective skin for humans.[15,16]

Additionally, in our daily life, the limited exposure of the human body to sunlight is essential for good health, as sunlight allows the body to produce vitamin D, which is essential for bone growth. However, sunlight also contains harmful ultraviolet (UV) radiation, which can harm the human body.[17] Depending on the wavelength, sunlight-based UV radiation can be divided into UV-A (320–400 nm), UV-B (280–320 nm), and UV-C (200–280 nm).[18,19] Thanks to the existence of the ozone layer as part of the earth's atmosphere, the majority of UV-C radiation is blocked; however, UV-B and UV-A radiation can still penetrate this layer, ultimately becoming the chief causes of many serious

Beijing Key Laboratory of Clothing Materials R&D and Assessment, Beijing Engineering Research Center of Textile Nanofiber, School of Materials Design & Engineering, Beijing Institute of Fashion Technology, Beijing 100029, China. E-mail: a.wujing@163.com; clyzxq@bift.edu.cn

† Electronic supplementary information (ESI) available: S1–S8. See DOI: 10.1039/d1ra07912c

conditions, such as skin hyperpigmentation, erythema, apoptotic cell death, skin cancer, and so on.[8,20–22] UV protection provided by ordinary clothing is not sufficient to protect human skin from damage due to UV radiation in some situations.[23] The effective protection of skin from the consequences of excessive exposure to sunlight-based UV radiation requires personal protective materials that are capable of absorbing or reflecting UV radiation before it reaches the skin surface.[24] In order to improve the UV protection abilities of clothing, considerable efforts have been made to fabricate UV protective materials. Xiao *et al.* deposited TiO_2 nanoparticles, which act as UV absorbers, *via* an atomic layer deposition technique, and the as-prepared samples showed excellent UV protection performance.[25] N. Abidi *et al.* reported a successful titania-nanosol coating on cotton fabrics, which imparted cotton fabric with excellent self-cleaning and UV protective properties.

Based on the current status of the field, research combining functional fabrics with comfort, allowing a full range of functionality and improving the wearing experience, is still in its infancy thus far. Herein, we fabricate polylactic acid (PLA) based Janus fabric, integrating directional moisture transport and UV protection abilities. PLA, as a kind of bio-based and biodegradable material, exhibits numerous advantages, such as excellent biocompatibility, good mechanical properties, and easy processability, making it a promising eco-friendly candidate for industrial applications that is compatible with human use.[26–28] In this work, inspired by the strong and long-lasting bio-adhesion of marine mussels in wet environments,[29] DOPA, with a molecular structure that mimics the single units of mussel adhesive protein, was used to directly anchor titanium dioxide nanoparticles (TiO_2) to the surface of PLA fabric during the TiO_2 sol–gel fabrication process, resulting in a TiO_2@PDA coating and endowing the PLA fabric with superhydrophilicity and a hierarchical rough surface (TiO_2@PDA–PLA). Subsequently, a thin layer of PLA fibrous membrane showing hydrophobicity was stacked on TiO_2@PDA–PLA *via* electrospinning (PLA-E). Thus, the PLA-E/TiO_2@PDA–PLA Janus membrane was successfully fabricated. Thanks to the asymmetric wettability and anchored TiO_2, this membrane exhibits efficient directional moisture transport and excellent UV protection abilities, and this may provide a new pathway for fabricating multifunctional personal protective materials with both versatility and biodegradability.

Experimental section

Materials

Polylactic acid (PLA, M_n = 47 000) was supplied by Zhejiang Haizheng Biomaterial Co. (Taizhou, China) and PLA fabric was obtained from Puyang Yurun New Material Co. (Puyang, China). Dopamine (98%) and tris-(hydroxymethyl)aminomethane (Tris) were received from Sigma-Aldrich (St. Louis, MO, USA). Tetrabutyl titanate (TBT) was bought from Shanghai Macklin Biochemical Co. (Shanghai, China). *N,N*-Dimethylformamide (DMF), dichloromethane (DCM), ethanol, sodium hydroxide (NaOH), and hydrochloric acid (73%) were purchased from Beijing Yili Fine Chemical Co. (Beijing, China). All chemicals

were of analytical grade and used as received without any further purification.

Fabrication of superhydrophilic TiO_2@PDA–PLA fabric

Firstly, the purified PLA fabric was cut into squares (8 cm × 8 cm) and rinsed ultrasonically using NaOH solution (10 g L^{-1}) for 3 h and water. 80 mg of dopamine hydrochloride was dispersed in 40 mL of tris(hydroxymethyl)aminomethane hydrochloride (Tris–HCl) solution (10 mM, pH = 8.5). The dried PLA(NaOH) fabric was immersed into the as-prepared solution for 24 h at 30 °C. After that, PDA–PLA fabric samples were obtained.

Then, the PDA–PLA fabric was immersed into 500 mL of ethanol. Titania nanoparticles (TiO_2) were prepared according to the classical sol–gel Stöber method. 20 mL of TBT was slowly dropped into the ethanol containing PDA–PLA fabric under stirring. The reaction was initiated upon the addition of deionized water (TBT : deionized water = 20 : 1 (v/v)). Hydrochloric acid was used to adjust the pH value to about 3. The above reaction mixture was stirred at 40 °C for 18 h. Finally, the resultant TiO_2@PDA–PLA fabric was rinsed with ethanol to remove residual TiO_2 nanoparticles and dried at 60 °C for 2 h.

Fabrication of hydrophobic polylactic acid electrospun (PLA-E) fibrous membranes

The above-fabricated TiO_2@PDA–PLA covered the drum (200 rpm) of the electrospinning set-up as the collector. PLA pellets were dissolved in DCM and DMF solvent (7 : 3 wt/wt) under magnetic stirring at 40 ± 5 °C for 6 h to obtain precursor solutions with concentrations of 5, 7.5, and 10 wt%. Nearly 3 mL of precursor solution was placed in a 5 mL syringe. During the electrospinning process, the distance between the collector and the spinning nozzle and the electrospinning voltage were set to about 15 cm and 18 kV, respectively. In order to obtain PLA-E fibrous membranes with different diameters, spinning nozzles with inner diameters of 0.6, 0.8, 1.0, and 1.2 mm (named 6G, 8G, 10G, and 12G, respectively) were used. The flow rate of the PLA solution was controlled between 0.03 mm min^{-1} and 0.08 mm min^{-1} using the syringe pump.

Fabrication of the Janus PLA-E/TiO_2@PDA–PLA membranes

Based on the above-mentioned fabrication process, PLA-E fibrous membranes were obtained *via* electrospinning and collected on the TiO_2@PDA–PLA fabric; Janus membranes were successfully obtained as a result.

Instruments and characterization

SEM images were taken using a field-emission scanning electron microscope (JSM-6700F, Tokyo, Japan). The average diameters of the PLA-E fibers were measured on the basis of SEM images. The water contact angles were measured using an OCA20 contact angle system (Dataphysics, Germany) at 25 °C. 5 μL of deionized water was dropped onto the surface and the average contact angle value was obtained *via* measuring at least five different positions for each sample. The chemical

compositions of the prepared samples were investigated *via* energy-dispersive X-ray spectroscopy (EDS IE300X, Oxford British) and Fourier-transform infrared spectrometry (FTIR) (Nicolet 8700, FT-IR spectrometry, Madison, WI, USA) in the wavenumber range from 400 to 4000 cm^{-1}. The thicknesses of the PLA-E fibrous membranes were adjusted *via* controlling the electrospinning time. TiO$_2$@PDA–PLA fabric with a fixed area (width $\times$ length = 10 cm $\times$ 10 cm) was used as the substrate. Then, PLA fibers were electrospun on the substrate for 1, 2, 3, 4, 5, 10, 14, 15, 20, 25, and 30 min, respectively. Thus, the membrane thickness can be adjusted *via* fixing the area of the substrate and changing the electrospinning time. A thickness gauge (CHY-U, Jinan, China) was used to measure the thicknesses of the Janus membranes. The directional water transport performance was quantitatively measured using a moisture-management tester (MMT) (SDL ATLAS, Ltd, Beijing, China). During the measurement process, the sample was put between two horizontal (top and bottom side) electrical sensors, and saline water (0.21 g $\pm$ 0.01 g, 0.9% NaCl in aqueous solution, 0.9 g of NaCl dissolved in 100 g of distilled water, molarity: 0.154 mol L^{-1}, based on AATCC TM195) was dropped onto the top surface of the samples over 20 s. The amounts of saline water on both the top and bottom surfaces of the sample can be calculated based on the corresponding resistance values (in the first 120 s after the saline water was dropped onto the surface). All samples were put into an environment-controlled room (21 $\pm$ 1 °C, relative humidity 65 $\pm$ 2%, refer to ASTM D1776) for at least 24 h prior to testing. The UV transmittance spectra of the prepared samples were obtained using an ultraviolet-visible spectrophotometer (PerkinElmer Lambda 950, USA). Spectra were recorded in the wavelength range from 200 nm to 600 nm at room temperature. The air permeability was measured using an automatic air permeability tester (YG461Z) with a pressure drop of 100 Pa. The water vapour transmission (WVT) of the Janus fabric membranes was investigated using YG601H computer-type fabric moisture permeability testing apparatus. The mechanical properties of the as-prepared samples were measured using a microcomputer-controlled electronic universal testing machine (TSE202A, Shenzhen WANCES Testing Machine Co., Ltd, China). The samples were cut to a size of 40 mm $\times$ 25 mm (length $\times$ width). The stretching velocity was 20 mm min^{-1}.

Results and discussion

The PLA-E/TiO$_2$@PDA–PLA Janus membrane with great asymmetric wettability was fabricated *via* electrospinning combined with *in situ* dopamine oxidative polymerization and a sol–gel method. Fig. 1 schematically illustrates the fabrication process. The PLA fabric was initially washed in NaOH solution and deionized water and dried for usage. Then, the above pre-treated PLA fabric was immersed in stirred tris(hydroxymethyl)aminomethane hydrochloride (Tris–HCl) aqueous solution (pH = 8.5), which contained dopamine. As seen in the strong and long-lasting bio-adhesion of marine mussels in wet environments, dopamine, a biotic molecule containing catechol and amine groups, can self-polymerize to form polydopamine

(PDA) in an alkaline environment based on aerobic auto-oxidation.[30,31] Taking advantage of strong covalent and non-covalent interactions with a surface, dopamine can form layers of "glue" on all kinds of material surfaces. We used this feature of dopamine polymerization to directly anchor TiO$_2$ nanoparticles to the surface of the PLA fabric. In a rapid sequence, tetrabutyl titanate (TBT) was added to the above solution dropwise. During the process of the synthesis of TiO$_2$ *via* a sol–gel method, TiO$_2$ nanoparticles were anchored *in situ* on the PLA fabric surface (TiO$_2$@PDA–PLA), showing super-hydrophilicity. After that, the TiO$_2$@PDA–PLA fabric was employed as a collector, on which another hydrophobic PLA fibrous membrane layer was deposited *via* electrospinning (PLA-E). Finally, upon peeling off the membrane from the electrospinning drum, a free-standing PLA-E/TiO$_2$@PDA–PLA Janus membrane with asymmetric wettability had been successfully fabricated.

A schematic diagram of the PLA-E/TiO$_2$@PDA–PLA Janus membrane is given in Fig. 2(a). SEM was applied to explore the morphologies of the two composited layers. Fig. 2(b) shows an SEM image of the TiO$_2$@PDA–PLA fabric. Compared with pristine PLA fabric (ESI S1†), it can be seen that the yarns of TiO$_2$@PDA–PLA fabric were roughly covered in a layer of nanoparticles/mastoids which overlapped densely, forming hierarchical polydisperse aggregates (an enlarged view is given in Fig. 2(c)).

Furthermore, the obtained TiO$_2$@PDA–PLA fabric shows a water contact angle (WCA) of 0° (inset of Fig. 2(b)). When a 5 μL water droplet was dripped onto TiO$_2$@PDA–PLA, it rapidly spread within 0.08 s (ESI S2†), indicating the presence of superhydrophilicity. Meanwhile, the influences of PDA and TiO$_2$@PDA on the wettability of PLA fabric were characterized (more details are given in ESI S2†). It is obvious that both PDA and TiO$_2$@PDA make PLA fabric superhydrophilic. The differences between the two in terms of wettability were mainly seen in the water spreading and absorbing time. A water droplet (5 μL) could fully spread and absorb on both TiO$_2$@PDA–PLA and PDA–PLA fabric within 1 s. However, the water spreading and absorbing time of TiO$_2$@PDA–PLA fabric was 0.08 s, which was much shorter than that of PDA–PLA fabric (0.84 s). On the other side, as seen in Fig. 2(d) and (e), PLA-E fibers with relatively smooth surfaces were randomly distributed on the collector with an average fiber diameter of about 482 nm (ESI S3†). The WCA of PLA-E was 118 $\pm$ 0.3°, indicating hydrophobicity (inset of Fig. 2(d)).

EDS analysis was carried out to uncover the chemical composition of the Janus membrane. When EDS analysis of the PLA-E layer of the Janus membrane was carried out (Fig. 2(f)), the content levels of C and O are 49.09% and 48.19%, respectively. A small amount of Ti was also detected, which is attributed to the thin PLA-E fibrous layer not completely covering the adjacent TiO$_2$@PDA–PLA layer. When EDS analysis was carried out from the TiO$_2$@PDA–PLA side (Fig. 2(g)), it can be seen that C, O, and Ti elements appear, and they are distributed on the fabric surface uniformly. Compared with pristine PLA fabric, which only contains C and O (ESI S4†), the appearance of Ti indicated that TiO$_2$ nanoparticles were successfully synthesized
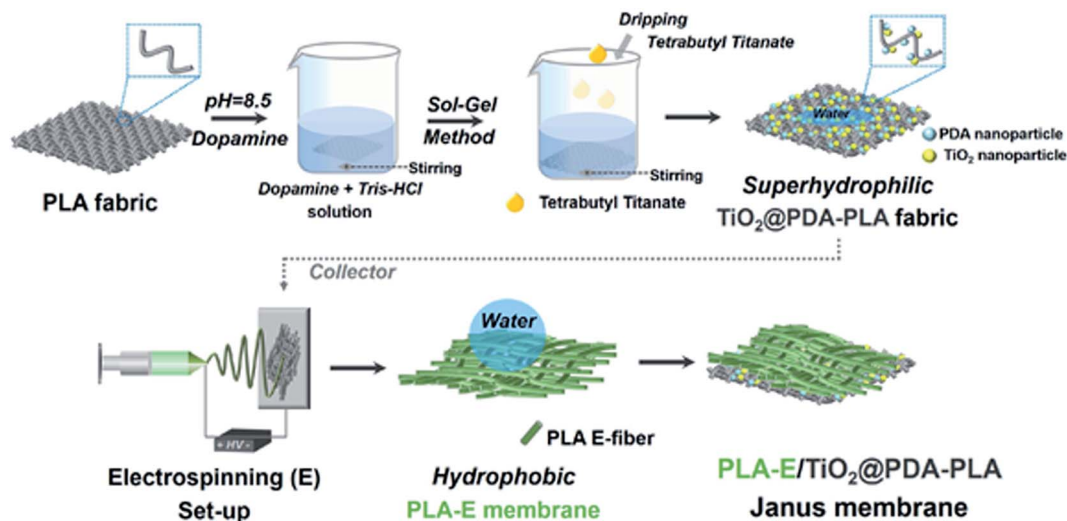
Fig. 1 A schematic illustration of the fabrication process of the PLA-E/TiO$_2$@PDA–PLA Janus fabric membrane with asymmetric wettability between its two sides. Superhydrophilic TiO$_2$@PDA–PLA fabric was prepared through dopamine oxidative polymerization and a sol–gel method based on pristine PLA fabric. After that, a hydrophobic PLA fibrous membrane layer was deposited onto the superhydrophilic TiO$_2$@PDA–PLA fabric. As a result, the Janus membrane was successfully obtained.

in situ via the sol–gel method and anchored on the PDA–PLA fabric. In addition, it is important to note that N attributed to PDA does not appear in EDS element mapping analysis due to its low content.

X-ray photoelectron spectroscopy (XPS) was used to verify the chemical components of as-prepared samples (Fig. 2(h)). The survey spectra indicated that PLA fabric, the PLA-E fibrous membrane, PDA–PLA, and TiO$_2$@PDA–PLA fabric contained the elements C and O. However, a new peak appeared in the survey spectrum of TiO$_2$@PDA–PLA fabric, which was attributing to the existence of Ti (from TiO$_2$). The high-resolution C 1s XPS spectra of PLA fabric, the PLA-E fibrous membrane, PDA–PLA, and TiO$_2$@PDA–PLA showed three peaks positioned at ~284.8 eV, 285–287 eV and 288–290 eV, which were assigned to C–C/C–H, C–O, and C=O.[32] For the PLA-E fibrous membrane, due to the spin-orbital coupling of electrons, the Ti 2p energy levels were decomposed into Ti 2p$_{1/2}$ and Ti 2p$_{3/2}$, with corresponding binding energies of 461.34 eV and 455.29 eV, indicating that TiO$_2$ was successfully anchored on the material.[33]

In addition, analysis of the wettability of the PLA-E fibrous membranes prepared using different types of electrospinning nozzles (difference in inner diameter), resulting in different average fiber diameters, was carried out. Water droplets of about 5 μL were allowed to contact the surfaces of the as-prepared samples. The water contact angles were 122.5° ± 0.8°, 116.4° ± 0.2°, 113.1° ± 0.1°, and 103.5° ± 0.7° for PLA-E(6G), PLA-E(8G), PLA-E(10G), and PLA-E(12G), respectively, indicating the PLA-E fibrous membranes are hydrophobic (inset photos in blue dotted frames in Fig. 3(a)). The natural properties of PLA and the porous structure of the PLA-E fibrous membrane, bestowing high surface roughness, are the main reasons for the hydrophobicity. It also can be seen that the average fiber diameter influenced the wettability. With a decrease in the average fiber diameter, the WCA of the PLA-E

fibrous membrane increased slightly; this is because for a fiber-based surface, a smaller fiber diameter usually brings about greater surface roughness, which can enhance or "enlarge" the wetting behaviour.[3,13,34] We further used Fourier-transform infrared spectroscopy (FTIR) to characterize the chemical compositions of the samples. As depicted in Fig. 3(b), the spectra of pure TiO$_2$ nanoparticles and TiO$_2$@PDA–PLA show that absorbed water and hydroxyl groups existed on the surfaces of the samples, as proved by the presence of the broad peak between 3750 and 3300 cm^{-1}. C=C resonance vibrations from aromatic rings and N–H bending vibrations were observed at 1613 cm^{-1} and 1509 cm^{-1}, respectively, indicating the presence of PDA.[35,36] An absorption peak was also found at around 662 cm^{-1}, which was assigned to the stretching vibrations of Ti–O–Ti bonds. In addition, for PDA–PLA and TiO$_2$@PDA–PLA samples, C=C resonance vibrations from aromatic rings and N–H bending vibrations were observed at 1613 cm^{-1} and 1509 cm^{-1}, which were the characteristic absorption peaks of polydopamine. Fig. 3(c) exhibits the water directional transport capabilities of the Janus membrane, defined as directional (yes) or non-directional (no), as a function of the electrospinning time. Here, water droplets were dripped on the hydrophobic PLA-E fibrous side. When the electrospinning time of PLA-E was less than 4 min, water droplets could transport from both sides of the Janus membrane. However, when the PLA electrospinning time was above 4 min but less than 14 min, water droplets could penetrate from the hydrophobic PLA-E fibrous membrane side to the superhydrophilic TiO$_2$@PDA–PLA fabric side of the Janus fabric membrane, but they were blocked in the reverse direction, exhibiting directional water transport. Upon continuing to increase the electrospinning time (above 14 min), water droplets were blocked from both sides.[7] Such unique one-way water transport capabilities can be attributed to the asymmetric wettability between the two sides of the Janus
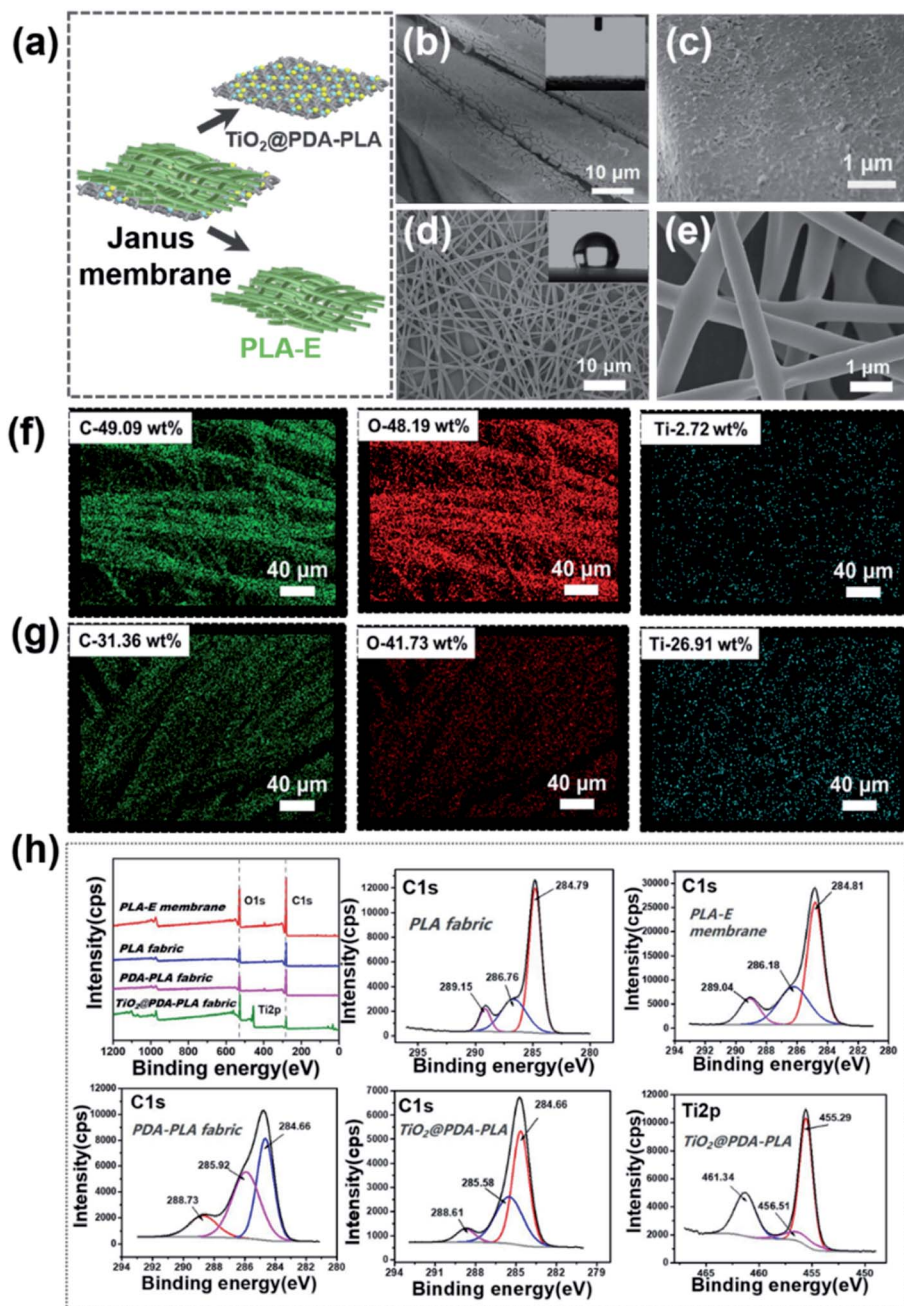
Fig. 2 (a) A schematic diagram of the PLA-E/TiO$_2$@PDA–PLA Janus membrane. (b) An SEM image of TiO$_2$@PDA–PLA fabric; the WCA is about 0° (inset), indicating superhydrophilicity. (c) A magnified view of the SEM image in (b). (d) An SEM image of the PLA-E fibrous membrane; the PLA-E fibrous membrane shows hydrophobicity, with a WCA of 118 ± 0.3° (inset). (e) A magnified view of the SEM image in (d). EDS element distribution maps of the Janus membrane measured from the (f) PLA-E membrane side and (g) TiO$_2$@PDA–PLA fabric side. (h) XPS analysis of PLA fabric, the PLA-E membrane, PDA–PLA fabric, and TiO$_2$@PDA–PLA fabric.

membrane. Thus, the hydrophobic layer should work to block the penetration of water, while the superhydrophilic layer favours transport.[6]

The mechanism is illustrated in Fig. 3(d). Water droplets were first dropped onto the hydrophobic PLA-E fibrous membrane side then onto the superhydrophilic TiO$_2$@PDA–PLA fabric side. Based on our previous research work, we found that for a Janus membrane with asymmetric wettability, once

the thickness of the superhydrophilic layer is fixed, the water transport capacity is highly dependent on the thickness of the hydrophobic layer.[14,37,38] Thus, in this work, the thickness of the superhydrophilic TiO$_2$@PDA–PLA fabric layer was fixed, and the thickness of the hydrophobic PLA-E fibrous membrane was adjusted based on the electrospinning time. The relationship between the electrospinning time of PLA and the thickness of the Janus membrane is shown in ESI S5.† When water contacted
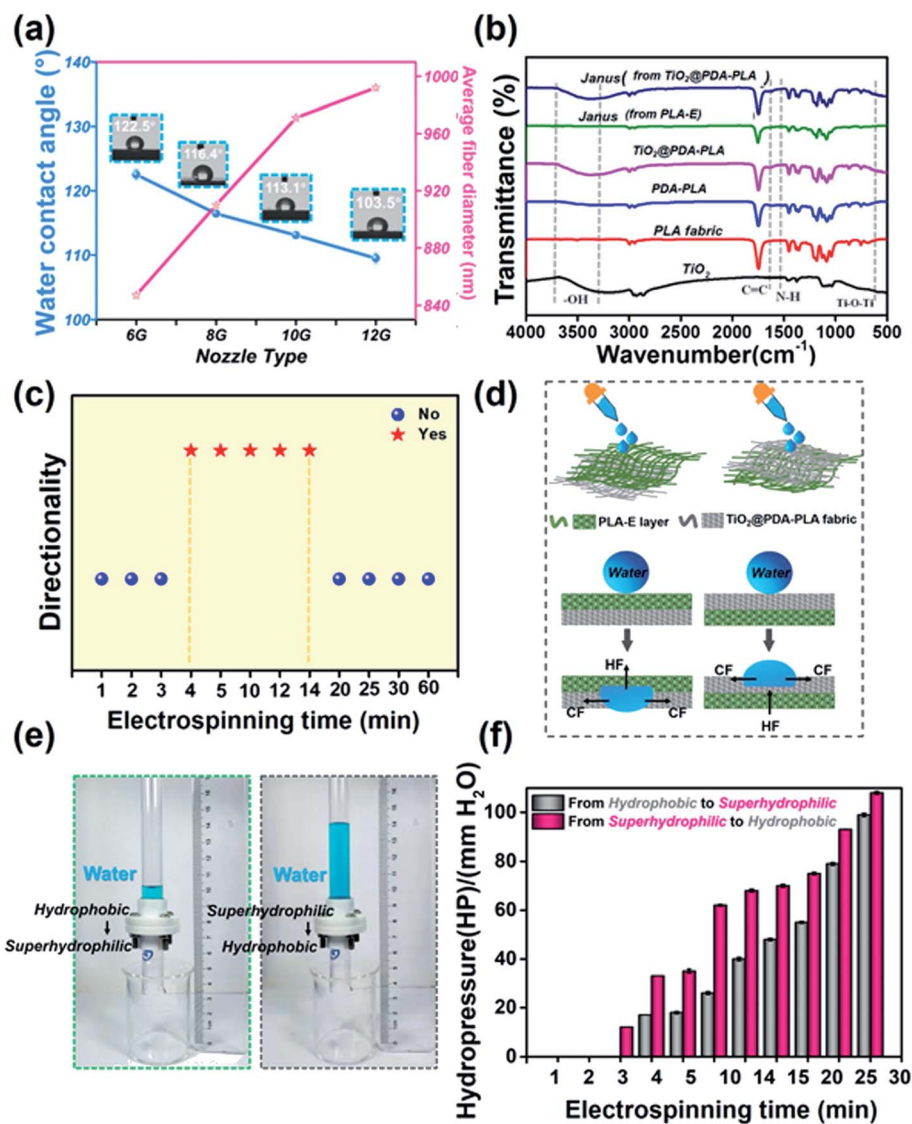
Fig. 3 (a) Water contact angles of PLA-E fibrous membranes prepared with different types of electrospinning nozzles, and the relationship between the wettability and the average fiber diameter of the PLA-E fibrous membranes. (b) FTIR spectra of the as-prepared samples. (c) The water transport capabilities of Janus membranes with different electrospinning times used for the PLA-E fibrous membrane. (d) A schematic illustration of the directional water transport mechanism of the Janus membrane with asymmetric wettability. (e) The critical breakthrough column height of water (HP) for the Janus fabric membrane in the hydrophobic PLA-E fibrous membrane (green dotted frames) and super-hydrophilic TiO$_2$@PDA–PLA fabric (gray dotted frames) direction. (f) The relationship between HP on both sides of the Janus fabric membrane *versus* the electrospinning time used for the PLA-E fibrous membrane.

the hydrophobic PLA-E surface, it is subjected to two opposite forces: so-called hydrostatic pressure (HP) generated by the water drop itself and hydrophobic force (HF) caused by the hydrophobic layer. HP supports water transport across the membrane, while HF resists water transport. HF is a constant value, which is determined by the use of a certain material. When water is dripped onto the membrane, on account of the accumulated water volume, the penetrative HP increases. Once the penetrative depth reaches the thickness of the PLA-E fibrous membrane, water contacts with the superhydrophilic TiO$_2$@-PDA–PLA fabric, where it is then subjected to capillary force (CF) as a result of the superhydrophilic membrane. Under the action of HP and CF, water droplets will be "dragged" through the

Janus membrane (Fig. 3(d), left). On the contrary, once water droplets contact the superhydrophilic TiO$_2$@PDA–PLA side, they tend to spread out into a thin water film or are absorbed by the superhydrophilic layer under the force of HP and CF. When water drops move to the interface between the PLA-E fibrous membrane and TiO$_2$@PDA–PLA fabric, HF will prevent water from further penetrating into the hydrophobic layer. Even if the water volume is increased to provide larger HP, water is much more inclined to spread over the superhydrophilic layer instead of penetrating through the hydrophobic layer (Fig. 3(d), right). A Janus membrane with this type of asymmetric wettability shows unidirectional water transport capabilities, like a "water diode",

allowing water transport from the hydrophobic to the superhydrophilic side but being blocked in the reverse direction.[39]

To demonstrate the effects of water on both sides of the Janus membrane in an in-depth manner, the hydrostatic pressure (HP) needed to make water pass through the porous channels of the membrane was measured. As shown in Fig. 3(e), HP values, from the hydrophobic PLA-E side to the superhydrophilic TiO_2@PDA–PLA side and in the reverse direction, were measured *via* fixing the area of the Janus fabric membrane, slowly dripping water droplets through a tubular container, and then recording the height of the water column at the time when water begins to penetrate. Fig. 3(f) shows the relationship between the PLA-E electrospinning time and the HP. It is noteworthy that HP from the hydrophobic PLA-E side to the superhydrophilic TiO_2@PDA–PLA side was much lower than that in the reverse direction (from TiO_2@PDA–PLA side to PLA-E, pink columns), indicating that it was easier for water droplets to transport from the hydrophobic side to the superhydrophilic side. When the electrospinning time of PLA-E increased, the HP increased correspondingly, which can be attributed to the thicker PLA-E fibrous membrane leading to longer hydrophobic channel lengths for water to break though, making it much more difficult for water to be transported.[40]

As an excellent type of fabric functionality that can guarantee human comfort, enhanced directional moisture transport is important for drying the human body. Fig. 4 quantitatively depicts moisture management testing (MMT) of the PLA-E/ TiO_2@PDA–PLA Janus membrane. Fig. 4(a) presents the water content on both sides of the Janus membrane as a function of the electrospinning time. During the MMT process, a total mass of 0.2 g of salt water was consistently dropped for 20 s, and water movement in the membrane was observed for 120 s. It was observed that when the electrospinning time of the top hydrophobic PLA-E fibrous membrane layer increased, the water content decreased then increased gradually. When the electrospinning time of PLA-E was 10 min, the water content reached its minimum value (the red dotted box, in Fig. 4(a)).

The reason for this phenomenon was that moisture was spontaneously transported across the Janus membrane from the hydrophobic PLA-E side to the superhydrophilic TiO_2@-PDA–PLA side. Once the electrospinning time of PLA-E was increased above 10 min, the increased thickness of PLA-E prevented directional moisture transport, causing water to accumulate in the hydrophobic PLA-E layer. In the same way, when the Janus membrane was reversed, placing the superhydrophilic TiO_2@PDA–PLA layer on top, the water content increased gradually and then tended to be constant. This phenomenon can be explained based on the fact that with an increase in the thickness of the hydrophobic PLA-E layer, water merely spread on the top superhydrophilic layer instead of penetrating through the Janus membrane, and finally the water content reached a constant value. In addition, it also can be seen that for the PLA-E/TiO_2@PDA–PLA Janus membrane, PLA-E with a smaller average fiber diameter has better directional moisture transport capabilities (ESI S6†).

Fig. 4(b) shows MMT images of the water content on the top and bottom surfaces of Janus membranes where water was dropped on the PLA-E and TiO_2@PDA–PLA sides, respectively. The dark regions represent non-wetted areas and the blue regions show wetted areas. High contrast is noticed between the "blue" and the "dark" areas, which confirms that most water is directionally transported to the superhydrophilic TiO_2@PDA–PLA layer and retained there. Subsequently, the directional moisture transport capabilities of the Janus fabric membrane from the hydrophobic to the superhydrophilic side and in the reverse direction have been measured, and the results are shown in Fig. 4(c). It is apparent that the directional moisture transport capabilities from the hydrophobic PLA-E side to the superhydrophilic TiO_2@PDA–PLA side of all the as-prepared Janus membranes with different PLA-E electrospinning times were higher than those in the reverse direction. It also can be seen that when the PLA-E electrospinning time was 10 min, the directional water transport capabilities reached their maximum value (pink dotted box in Fig. 4(c)), that is, 403.5% from the hydrophobic side to the superhydrophilic side, and −595% from the superhydrophilic side to the hydrophobic side.

To investigate the UV resistance of the as-prepared samples, the UV-vis transmittance was measured over a wavelength range
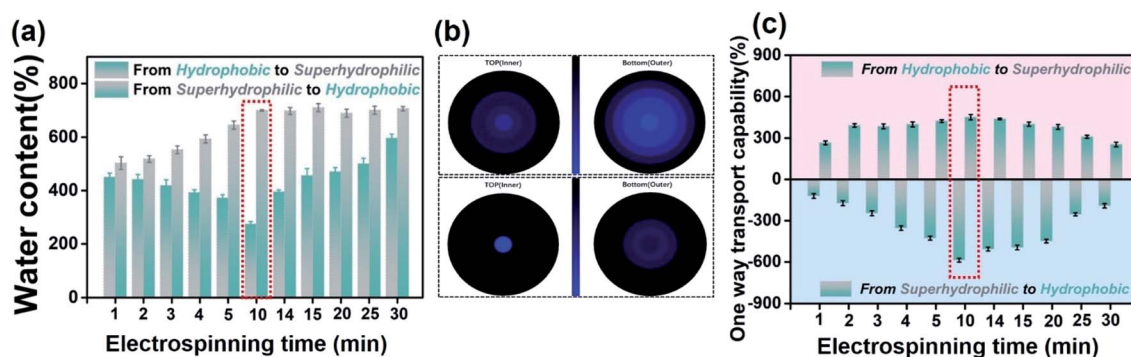

Fig. 4 (a) Moisture-management testing (MMT) results for Janus membranes fabricated with different PLA-E electrospinning times. (b) MMT images exhibiting water diffusion on Janus fibrous membranes at the top and the bottom when the PLA electrospinning time was 10 min: top row, TiO_2@PDA–PLA on top; bottom row, PLA-E on top. (c) Measurements of the one-way transport capabilities of the as-prepared Janus membranes.

of 250–400 nm, which is the most harmful to humans. Fig. 5(a) and (b) shows the UV-transmission spectra and UV-B transmittance, respectively, for all as-prepared samples. Based on a large number of literature reports, titanium dioxide, which is toxin- and odor-free, shows excellent shielding effectiveness against UV radiation, and it does not decompose or become discolored after absorbing UV light, exhibiting long-lasting UV-blocking effects.[41–43] Accordingly, the UV protection performance of TiO$_2$@PLA fabric (TiO$_2$ anchored on PLA fabric without PDA) was tested. It can be seen that the UV protection capabilities were improved compared with pristine PLA fabric, but the effects were not particularly ideal, mainly because of the poor adhesion of TiO$_2$ nanoparticles to the surface of PLA fabric without the PDA "glue layer". Then, we investigated the UV protection abilities of PDA–PLA fabric and TiO$_2$@PDA–PLA fabric. It was found that UV-B transmission can be reduced to below 20% upon constructing a solid TiO$_2$@PDA nanostructure on the surface of PLA fabric. This can be explained as follows: (i) the molecular structure of PDA is similar to that of melanin in organisms, which has good absorption capabilities toward light, ultraviolet light, and infrared light; and (ii) as an inorganic anti-UV agent, TiO$_2$ nanoparticles can absorb UV light to produce electron/hole pairs, with a scattering effect toward ultraviolet rays.[18,44,45] In addition, both sides of the Janus membrane have the same UV protection abilities. Thus, taking advantage of the absorbing and scattering of UV rays, the TiO$_2$@PDA nanostructure can effectively improve the UV protection abilities of the Janus membrane.

In light of practical applications, not only is excellent UV protection performance important, but good moisture and air permeability, ensuring comfort, play important roles in the development of a wearable fabric.[46] Fig. 5(c) shows the air permeability of the Janus membrane as a function of the electrospinning time. The air permeability of the membrane decreased as the PLA-E electrospinning time was increased, which is consistent with previous research.[47] Membranes that show lower air permeability can prevent aerosols, gases, and wind from reaching the human body.[48] Fig. 5(d) shows the relationship between the water vapor transmission (WVT) rate of the Janus fabric membrane and the PLA-E electrospinning time. The following points are notable. (i) With an increase in the PLA-E electrospinning time, the WVT rate of the Janus membrane shows a downward trend. This can be attributed to a longer electrospinning time leading to the denser accumulation of PLA-E nanofibers, blocking the pores and channel of the fibrous membrane. The morphologies of cross-sections of Janus membranes with different PLA-E electrospinning times and their corresponding porosities are shown in ESI S7.† (ii) The WVT rates when water vapor transmission was from the PLA-E side (inner side, close to human skin when worn) to the TiO$_2$@PDA–PLA side (outer side, away from human skin when worn) were higher than in the reverse direction for all the as-prepared membranes. This is of cardinal significance, because a normal adult loses 700–1200 g of sweat each day in a passive state (insensible perspiration) and 1200–2000 g of sweat each day in motion (sensible perspiration). When the moisture transmission of the fabric reaches 2200 g^{-2} d^{-1}, this can ensure
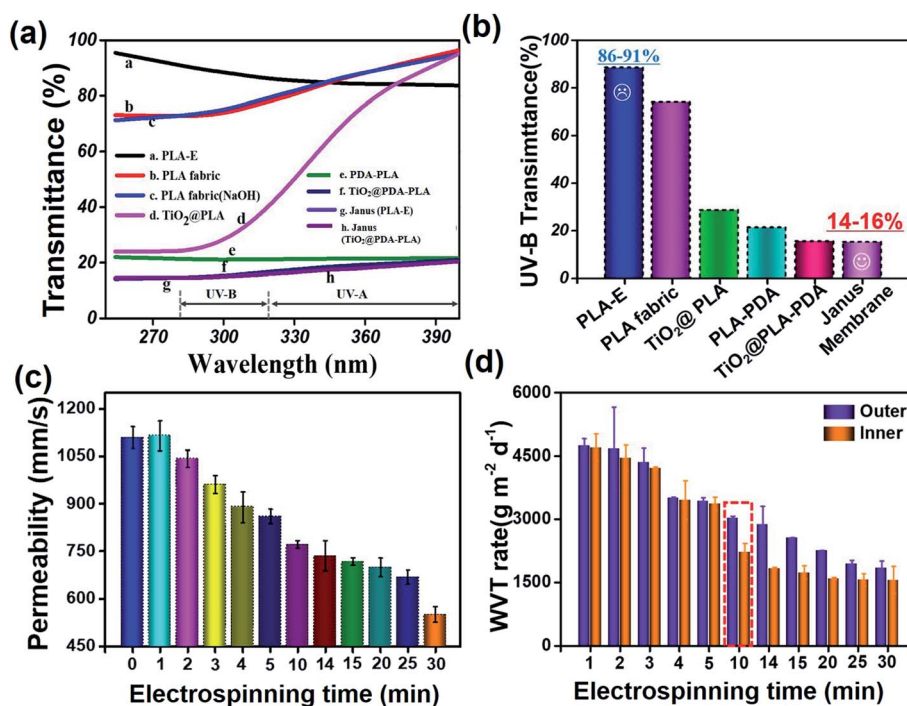

Fig. 5 (a) The UV transmission spectra of the as-prepared samples. (b) A histogram showing the UV-B transmittance levels of the as-prepared samples. The air permeabilities (c) and water vapour transmission (WVT) rates (d) of PLA-E/TiO$_2$@PDA–PLA Janus fabric membranes with different PLA-E electrospinning times.

the comfortable wearing of clothing. When the electrospinning time reached 10 min, the WVT rate of the Janus membrane (outer) is 3034 $g^{-2} d^{-1}$, much higher than 2200 $g^{-2} d^{-1}$ (the area marked in red dotted lines in Fig. 5(d)). Also, the mechanical properties of the membrane can meet the basic needs of clothing (ESI S8†). The better water vapor transmittance permeability can keep the human body dry and comfortable, making this Janus membrane a good candidate to act as a clothing fabric with excellent UV-protection abilities and efficient moisture transport capabilities.

Conclusions

In summary, we have successfully fabricated hydrophobic/superhydrophilic Janus fabric membranes based on green eco-friendly PLA *via* electrospinning combined with oxidative polymerization and sol–gel methods. Taking advantage of the great asymmetric wettability, the Janus fabric membranes show excellent directional moisture transport capabilities. In addition, due to the anchored TiO_2 nanoparticles, the Janus fabric membranes also show enhanced UV protection, exhibiting good functionality and attractive levels of comfort for wearing. This work can lay great foundations for the development of multifunctional personal protective materials.

Author contributions

J. Wu, X. Zhang, and R. Wang offered the idea and designed the experiments. Y. Gu, H. Pi, and J. Wu performed the experiments and analysed the experimental data. M. Hu helped to analyse the data. J. Wu and X. Zhang guided the study and revised the manuscript.

Conflicts of interest

There are no conflicts to declare.

Acknowledgements

Notes and references

1 Y. Zhang, W. Tian, L. Liu, W. Cheng, W. Wang, K.-M. Liew, B. Wang and Y. Hu, *Chem. Eng. J.*, 2019, **372**, 1077–1090.

2 A. Zhang, H. Zhao, J. Cheng, M. Li, S. Li and M. Gao, *Chem. Eng. J.*, 2021, **410**, 128361.

3 Y. Gao, Y. Wang, T. Yue, Y. Weng and M. Wang, *J. Colloid Interface Sci.*, 2021, **582**, 112–123.

4 X. Zhang, X. Wang, Z. Lei, L. Wang, M. Tian, S. Zhu, H. Xiao, X. Tang and L. Qu, *ACS Appl. Mater. Interfaces*, 2020, **12**, 14459–14467.

5 A. K. Yetisen, H. Qu, A. Manbachi, H. Butt, M. Dokmeci, J. P. Hinestroza, M. Skorobogatiy, A. Khademhosseini and S. H. Yun, *ACS Nano*, 2016, **10**, 3042–3068.

6 A. A. Babar, D. Miao, N. Ali, J. Zhao, X. Wang, J. Yu and B. Ding, *ACS Appl. Mater. Interfaces*, 2018, **10**, 22866–22875.

7 D. Miao, X. Wang, J. Yu and B. Ding, *Adv. Funct. Mater.*, 2021, 2008705.

8 H. X. Wang, J. Ding, L. M. Dai, X. G. Wang and T. Lin, *J. Mater. Chem.*, 2010, **20**, 7938–7940.

9 H. Zhou, H. X. Wang, H. T. Niu and T. Lin, *Sci. Rep.*, 2013, **3**, 2964–2970.

10 M. Y. Cao, J. S. Xiao, C. M. Yu, K. Li and L. Jiang, *Small*, 2015, **11**, 4379–4384.

11 B. Bai, K. Li, L. X. Shi, X. Z. Wan, X. Liu, F. L. Zhang, L. Jiang and S. T. Wang, *Adv. Mater.*, 2019, **31**, 1904113–1904119.

12 J. Wu, N. Wang, L. Wang, H. Dong, Y. Zhao and L. Jiang, *Soft Matter*, 2012, **8**, 5996–5999.

13 S. Tang, H. Pi, Y. Zhang, J. Wu and X. Zhang, *Appl. Sci.*, 2019, 3302.

14 B. Ren, H. Pi, X. Zhao, M. Hu, X. Zhang, R. Wang and J. Wu, *Nanoscale*, 2021, **13**, 9354–9363.

15 A. Mukhopadhyay and V. K. Midha, *J. Ind. Text.*, 2008, **37**, 225–262.

16 A. Mukhopadhyay and V. K. Midha, *J. Ind. Text.*, 2008, **38**, 17–41.

17 F. R. Gruijl, H. J. C. M. Sterenborg, P. D. Forbes, R. E. Davies, C. Cole, G. Kelfkens, H. Weelden, H. Slaper and J. C. Leun, *Cancer Res.*, 1993, **53**, 53–60.

18 S. Dadvar, H. Tavanai and M. Morshed, *J. Nanopart. Res.*, 2011, **13**, 5163–5169.

19 F. Ge, Y. Y. Ding, L. Yang, Y. Huang, L. Jiang and Y. Dan, *RSC Adv.*, 2015, **5**, 70473–70481.

20 S. E. Ullrich, *Mutat. Res.*, 2005, **571**, 185–205.

21 Q. Y. Wei, J. E. Lee, J. E. Gershenwald, M. I. Ross, P. F. Mansfield, S. S. Strom, L. E. Wang, Z. Z. Guo, Y. W. Qiao, C. I. Amos, M. R. Spitz and M. Duvic, *J. Natl. Cancer Inst.*, 2003, **95**, 308–315.

22 K. M. Hanson and J. D. Simon, *Proc. Natl. Acad. Sci. U. S. A.*, 1998, **95**, 10576–10578.

23 S. Mondal and J. L. Hu, *J. Appl. Polym. Sci.*, 2007, **103**, 3370–3376.

24 N. Abidi, L. Cabrales and E. Hequet, *ACS Appl. Mater. Interfaces*, 2009, **1**, 2141–2146.

25 X. F. Xiao, X. Liu, F. X. Chen, D. Fang, C. H. Zhang, L. J. Xia and W. L. Xu, *ACS Appl. Mater. Interfaces*, 2015, **7**, 21326–21333.

26 C. X. Zhu, W. Jiang, J. L. Hu, P. Sun, A. M. Li and Q. X. Zhang, *ACS Appl. Polym. Mater.*, 2020, **2**, 2509–2516.

27 A. A. Singh, M. E. Genovese, G. Mancini, L. Marini and A. Athanassiou, *ACS Sustainable Chem. Eng.*, 2020, **8**, 4128–4136.

28 J. W. Shi, L. Zhang, P. Xiao, Y. J. Huang, P. Chen, X. F. Wang, J. C. Gu, J. W. Zhang and T. Chen, *ACS Sustainable Chem. Eng.*, 2018, **6**, 2445–2452.

29 J. H. Waite and M. L. Tanzer, *Science*, 1981, **212**, 1038–1040.

30 J. K. Ryu, S. H. Ku, H. Lee and C. B. Park, *Adv. Funct. Mater.*, 2010, **20**, 2132–2139.

31 Y. L. Liu, K. L. Ai and L. H. Lu, *Chem. Rev.*, 2014, **114**, 5057–5115.

32 H. W. Zhang, Q. J. Niu, N. Wang, J. Nie and G. P. Ma, *Eur. Polym. J.*, 2015, **71**, 440–450.

33 D. A. Torres-Ceron, S. Amaya-Roncancio, J. S. Riva, A. Varagas-Eudor, D. Escobar-Rincon and E. Restrepo-Parra, *Surf. Coat. Technol.*, 2021, **421**, 127437.

34 H. X. Wang, J. Ding, L. M. Dai, X. G. Wang and T. Lin, *J. Mater. Chem.*, 2010, **20**, 7938–7940.

35 Y. L. Bai, Z. H. Li, B. W. Cheng, M. L. Zhang and K. M. Su, *RSC Adv.*, 2017, **7**, 21758–21767.

36 Y. L. Kang, J. Zhang, G. Wu, M. X. Zhang, S. C. Chen and Y. Z. Wang, *ACS Sustainable Chem. Eng.*, 2018, **6**, 11783–11792.

37 X. L. Tian, J. Li and X. Wang, *Soft Matter*, 2012, **8**, 2633–2637.

38 J. Wu, H. Zhou, H. Wang, H. Shao, G. Yan and T. Lin, *Adv. Mater. Interfaces*, 2019, 1801529.

39 L. L. Hou, N. Wang, X. K. Man, Z. M. Cui, J. Wu, J. C. Liu, S. Li, Y. Gao, D. M. Li, L. Jiang and Y. Zhao, *ACS Nano*, 2019, **13**, 4124–4132.

40 X. L. Tian, H. Jin, J. N. Sainio, R. H. A. Ras and O. Ikkala, *Adv. Funct. Mater.*, 2014, **24**, 6023–6028.

41 F. A. Grant, *Rev. Mod. Phys.*, 1959, **31**, 646–674.

42 K. H. Qi and J. H. Xin, *ACS Appl. Mater. Interfaces*, 2010, **2**, 3479–3485.

43 E. Ukaji, T. Furusawa, M. Sato and N. Suzuki, *Appl. Surf. Sci.*, 2007, **254**, 563–569.

44 Z. Wang, Y. Zhou, Y. W. Li and Y. Y. Cheng, *Small*, 2020, **16**, 1907042–1907062.

45 Y. K. Kim and D. H. Min, *Nanoscale*, 2013, **5**, 3638–3642.

46 X. Y. Gu, N. Li, H. H. Gu, X. Xia and J. Xiong, *J. Appl. Polym. Sci.*, 2018, 46360–46369.

47 S. Lee and S. K. Obendorf, *J. Text. Inst.*, 2007, **98**, 87–97.

48 A. Sadighzadeh, M. Valinejad, A. Gazmeh and B. Rezaiefard, *Polym. Eng. Sci.*, 2016, **56**, 143–149.